Monthly Notices of the ROYAL ASTRONOMICAL SOCIETY

MNRAS **473,** 4932–4936 (2018) doi:10.1093/mnras/stx2652
Advance Access publication 2017 October 11

Projected bounds on ALPs from *Athena*

Joseph P. Conlon, Francesca Day, Nicholas Jennings,★ Sven Krippendorf and Francesco Muia

Rudolf Peierls Centre for Theoretical Physics, 1 Keble Road, Oxford, OX1 3NP, UK

Accepted 2017 October 9. Received 2017 October 8; in original form 2017 July 24

ABSTRACT

Galaxy clusters represent excellent laboratories to search for axion-like particles (ALPs). They contain magnetic fields which can induce quasi-sinusoidal oscillations in the X-ray spectra of active galactic nuclei situated in or behind them. Due to its excellent energy resolution, the X-ray Integral Field Unit instrument on board the *Athena* X-ray Observatory will be far more sensitive to ALP-induced modulations than current detectors. As a first analysis of the sensitivity of *Athena* to the ALP–photon coupling $g_{a\gamma\gamma}$, we simulate observations of the Seyfert galaxy NGC 1275 (hosting the radio source 3C 84) in the Perseus cluster using the SIXTE simulation software. We estimate that for a 200 ks exposure, a non-observation of spectral modulations will constrain $g_{a\gamma\gamma} \lesssim 1.5 \times 10^{-13}\mathrm{GeV}^{-1}$ for $m_a \lesssim 10^{-12}\mathrm{eV}$, representing an order of magnitude improvement over constraints derived using the current generation of satellites.

Key words: astroparticle physics – elementary particles – galaxies: clusters: individual: Perseus.

1 INTRODUCTION

X-ray astronomy provides a novel arena for fundamental physics. Thanks to exciting recent data, such as the observed excess at 3.5 keV (Boyarsky et al. 2014; Bulbul et al. 2014), there has been a renewed interest among particle physicists in the great promise of X-ray astronomy to shed light on physics beyond the Standard Model, including the existence of new particles.

One area for which X-ray astronomy is particularly suitable is in the search for axion-like particles (ALPs). ALPs are light pseudo-scalars that are a well-motivated extension of the Standard Model (Peccei & Quinn 1977; Weinberg 1978; Wilczek 1978) that arise generically in string compactifications, for example see Conlon (2006), Svrcek & Witten (2006) and Cicoli et al. (2012). A general review of ALPs is Ringwald (2012). In the presence of a magnetic field $\langle B \rangle$, ALPs and photons interconvert (Sikivie 1983; Raffelt & Stodolsky 1988), and this induces quasi-sinusoidal oscillations at X-ray energies in the spectra of sources in and around galaxy clusters (Wouters & Brun 2013; Conlon, Powell & Marsh 2016).

Searches for these oscillations can be used to constrain ALP parameter space. Current constraints on ALPs derived in this fashion (Wouters & Brun 2013; Conlon et al. 2017; Berg et al. 2017; Marsh et al. 2017) are based on data taken with CCD detectors, which have an energy resolution of $\mathcal{O}(100\,\mathrm{eV})$. A large improvement with sensitivity will be achieved once data become available from microcalorimeters with $\mathcal{O}$(a few eV) energy resolution. Such microcalorimeters will be on board the Advanced Telescope for High ENergy Astrophysics (ATHENA), currently scheduled to launch in 2028. Its X-IFU instrument will have large effective area, good imaging and energy resolution of ∼2.5 eV, greatly enhancing the discovery potential for ALPs.

In this paper, we provide a first estimate for the experimental sensitivity of *Athena* to ALPs. We do so using simulated data for a mock observation of NGC 1275, hosting the radio source 3C 84, which contains the central AGN of the Perseus cluster. This object was chosen as we have previously used it to place bounds on ALPs using *Chandra* data (Berg et al. 2017).

2 REVIEW OF ALP–PHOTON INTERCONVERSION IN CLUSTERS

An ALP a couples to electromagnetism through the Lagrangian term:

$$L = \frac{1}{4M} a F_{\mu\nu} \tilde{F}^{\mu\nu} = \frac{1}{M} a \boldsymbol{E} \cdot \boldsymbol{B}, \tag{1}$$

where $M^{-1} = g_{a\gamma\gamma}$ parametrizes the strength of the interaction, and $\boldsymbol{E}$ and $\boldsymbol{B}$ are the electric and magnetic fields, respectively. As their potential and interactions are protected by shift symmetries, ALPs can naturally have very small masses m_a. The probability of ALP–photon interaction in the presence of an external magnetic field $\langle B \rangle$ is a standard result (Sikivie 1983; Raffelt & Stodolsky 1988).

★ E-mail: nicholas.jennings@physics.ox.ac.uk

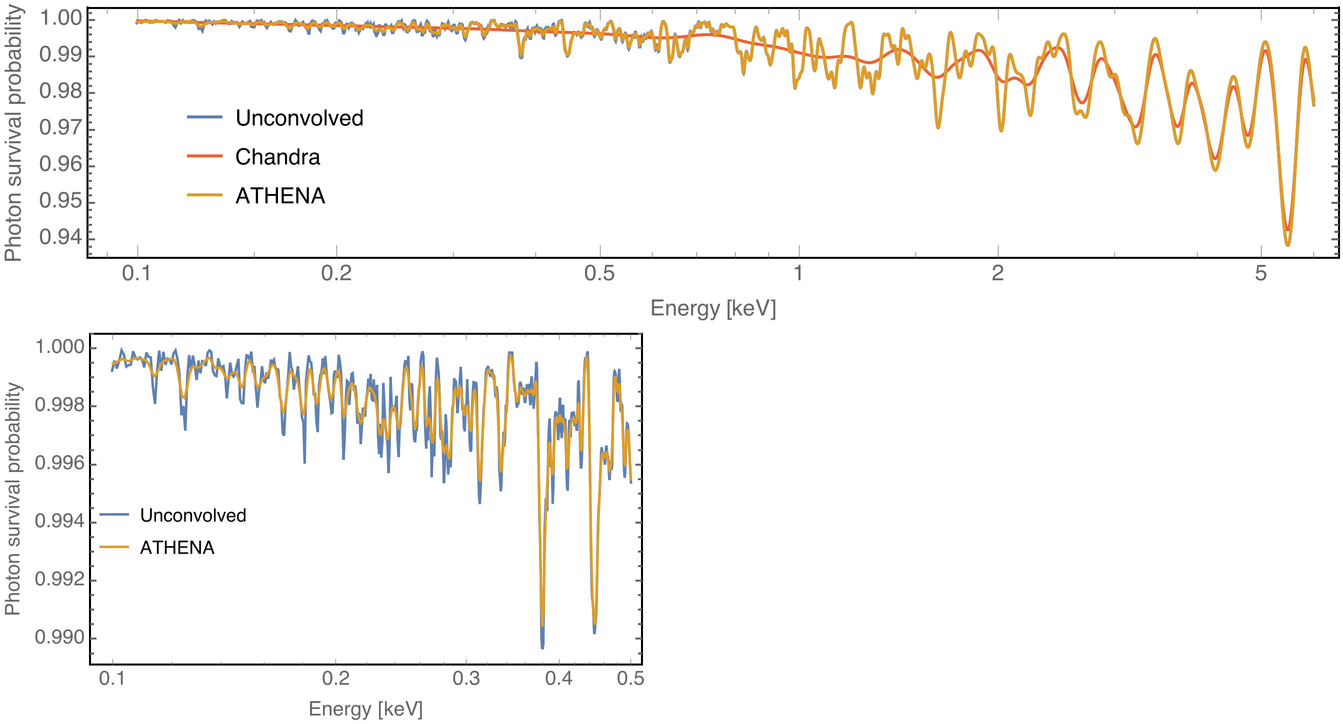

Figure 1. Above – a randomly generated photon survival probability along the line of sight from NGC 1275 to us: unconvolved (blue), convolved with a Gaussian with full width at half-maximum 150 eV [a typical energy resolution of *Chandra*'s ACIS-I detector (red)] and 2.5 eV for *Athena*'s X-IFU detector (orange). A central magnetic field of $B_0 = 25\,\mu$G was used, with a radial scaling of $B \sim n_{\rm e}^{0.7}$, further details in Section 4. The ALP–photon coupling is $g_{a\gamma\gamma} = 5 \times 10^{-13}\mathrm{GeV}^{-1}$. Small, rapid oscillations at low energies, and larger oscillations at high energies, are generic features of these survival probabilities. At energies < 2 keV, *Chandra* is unable to resolve oscillations while *Athena* performs much better. Left – the same photon survival probabilities, showing the sensitivity of X-IFU to oscillations at low energies.

The full analytic expression for the probability of an ALP being converted to a photon after propagating through a single magnetic field domain of length L is:

$$P_{a\to\gamma} = \frac{1}{2}\frac{\Theta^2}{1+\Theta^2}\sin^2\left(\Delta\sqrt{1+\Theta^2}\right), \tag{2}$$

where

$$\Theta = 0.28\left(\frac{B_\perp}{1\,\mu\mathrm{G}}\right)\left(\frac{\omega}{1\,\mathrm{keV}}\right)\left(\frac{10^{-3}\mathrm{cm}^{-3}}{n_{\rm e}}\right)\left(\frac{10^{11}\mathrm{GeV}}{M}\right), \tag{3}$$

$$\Delta = 0.54\left(\frac{n_e}{10^{-3}\mathrm{cm}^{-3}}\right)\left(\frac{L}{10\,\mathrm{kpc}}\right)\left(\frac{1\mathrm{keV}}{\omega}\right). \tag{4}$$

Here, $B_\perp$ denotes the magnetic field component perpendicular to the ALP wave vector, ω is the energy and $n_{\rm e}$ is the electron density. In the limit $\Delta, \Theta \ll 1$, $P \propto B^2L^2/M^2$. However, when $\Theta < 1$ but $\Delta > 1$, then $P \propto \Theta^2\sin^2\Delta$. This probability grows with energy, containing oscillations that are rapid at low energies and broader at higher energies. These oscillations leave a distinctive imprint on otherwise featureless spectra, and their absence allows us to constrain $g_{a\gamma\gamma}$.

This photon–ALP interconversion is particularly efficient in galaxy clusters (see e.g. Burrage et al. 2009; Conlon & Marsh 2013). Clusters have $\boldsymbol{B}$ fields of order $\sim\mu$G which extend over megaparsec scales, within which the magnetic field coherence lengths reach tens of kiloparsecs. The relatively low electron densities ($\sim 10^{-3}\mathrm{cm}^{-3}$) also imply that it is at X-ray energies that the 'sweet spot' of large Δ, small Θ and quasi-sinusoidal energy-dependent $P_{\gamma\leftrightarrow a}$ is located (Conlon & Marsh 2013; Wouters & Brun 2013; Angus et al. 2014; Conlon et al. 2016).

The 3D structure of intracluster magnetic fields is in general not known and so the precise form of the survival probability along any single line of sight cannot be determined. Fig. 1 illustrates the energy-dependent survival probability for a photon passing across 300 domains of a magnetic field, with the direction of the magnetic field randomized within each domain. The electron density and magnetic field strength in the model are based on those applicable in the Perseus cluster, but the pattern of smaller, rapid oscillations at low energies and slow oscillations with greater amplitude at high energies is generic.

AGNs situated in or behind galaxy clusters provide excellent X-ray sources to search for such spectral modulations. One outstanding example is the bright central AGN of the Perseus cluster, at the heart of the galaxy NGC 1275. Its intrinsic spectrum is well described by an absorbed power law (Churazov et al. 2003; Balmaverde, Capetti & Grandi 2006; Yamazaki et al. 2013; Fabian et al. 2015), and dominates the background cluster emission. The central cluster magnetic field value is estimated at $\sim 25\,\mu$G by (Taylor et al. 2006).

An analysis of archival data of observations of NGC 1275 by the *Chandra* and *XMM–Newton* satellites was done in Berg et al. (2017) (see Ajello et al. 2016 for a related analysis of NGC 1275 in gamma-rays). Extending methods pioneered in (Wouters & Brun 2013), the constraint on the ALP–photon coupling $g_{a\gamma\gamma} \lesssim 1.5 \times 10^{-12}\mathrm{GeV}^{-1}$ was found. For M87, a similar treatment was performed in Marsh et al. 2017, finding a bound $g_{a\gamma\gamma} \lesssim 1.5 \times 10^{-12}\mathrm{GeV}^{-1}$. An analysis of *Chandra* data of other bright point sources in galaxy clusters was conducted in (Conlon et al. 2017), deriving bounds of $g_{a\gamma\gamma} \lesssim 1.5 \times 10^{-12}\mathrm{GeV}^{-1}$ (for the Seyfert galaxy 2E 3140) and $g_{a\gamma\gamma} \lesssim 2.4 \times 10^{-12}\mathrm{GeV}^{-1}$ (for the AGN NGC 3862).

Table 1. Parameters taken from the *Athena* Mission Proposal and the *Chandra* Proposer's Guide.

	Athena (X-IFU)	*Chandra* (ACIS-I)
Energy range	0.2–12 keV	0.3–10 keV
Energy resolution at 6 keV	2.5 eV	150 eV
Spatial resolution	5 arcsec	0.5 arcsec
Time resolution	10 µs	0.2 s (2.8 ms single row)
Effective area	$2\ \mathrm{m}^2$ @ 1 keV	$600\ \mathrm{cm}^2$ @ 1.5 keV

These bounds all hold for light ALPs with masses $m_a \lesssim 10^{-12}$eV. This implies that these methods are not sensitive to an ordinary QCD (quantum chromodynamics) axion, which for a photon couplings $g_{a\gamma\gamma} \sim 10^{-12}\mathrm{GeV}^{-1}$ would typically have $m_a \sim 10^{-3}$eV. However, unconventional models for the QCD axion where the photon coupling is significantly enhanced compared to naive expectation may be constrained using these techniques.

The bounds produced are superior to the bound on light ALPs derived from SN 1987A of $g_{a\gamma\gamma} < 5 \times 10^{-12}\mathrm{GeV}^{-1}$ (Payez et al. 2015), and are similar to those projected for IAXO in this low mass region (Irastorza et al. 2012). The bounds are also superior to those inferred from the absence of cosmic microwave background (CMB) distortions in COBE FIRAS data (Mirizzi, Redondo & Sigl 2009), which constrain the product $g_{a\gamma\gamma}B < 10^{-11}\mathrm{GeV}^{-1}$nG. Here, B is the strength of the cosmic magnetic field, which is limited to $B <$ nG.

One major limiting constraint on existing data is the energy resolution of the detectors. If they exist, ALPs provide oscillatory structure all the way down to the lowest energies. However, as illustrated in Fig. 1, detectors with energy resolutions of $\mathcal{O}$(100eV) cannot resolve this structure at lower energies – but this does become accessible once a resolution of $\mathcal{O}$(2.5eV) is achieved. We now discuss the future *Athena* X-ray observatory, whose greatly enhanced technical capabilities offer improved sensitivity to ALP–photon interconversion.

3 ATHENA

The ATHENA is an ESA mission to explore the Hot and Energetic Universe, due to launch in 2028 (Nandra et al. 2013). The mirror will have a $2\ \mathrm{m}^2$ effective area and a 5 arcsec angular resolution. There are two instruments: the X-ray Integral Field Unit (X-IFU) and the Wide Field Imager (WFI). Here, we focus on the former, which will consist of an array of TiAu Transition Edge Sensor (TES) micro-calorimeters sensitive to the energy range 0.2–12 keV (Barret et al. 2016). When operated at a temperature of 50 mK, these can achieve an energy resolution of 2.5 eV below 7 keV (Gottardi et al. 2014), implying X-IFU will be able to resolve narrow spectral oscillations. A readout time of ∼10µs will ensure pile-up contamination is minimized. Table 1 contains a summary of its properties, taken from the *Athena* Mission Proposal[1], compared to properties of the *Chandra* ACIS-I detector, taken from the *Chandra* Proposer's Guide[2].

The combination of larger effective area, greatly improved energy resolution and reduced pile-up contamination means *Athena* has far more potential to detect ALP-induced oscillations than the best current satellites. The aim of this paper is to make the first quantitative estimate of the extent to which *Athena* will be able to improve constraints on $g_{a\gamma\gamma}$.

4 ESTIMATE OF PROJECTED BOUNDS

In terms of estimating bounds on $g_{a\gamma\gamma}$, we use the same method as previously applied with *Chandra* data (Berg et al. 2017). This allows for a direct comparison between the capabilities of *Chandra* and *Athena* in terms of placing bounds.

We simulate *Athena* observations of NGC 1275, using two models for the photon spectra of the AGN. The first is a standard spectrum without ALPs, and the second is a model with the same spectrum multiplied with the photon survival probability distribution as introduced in Section 2. Using simulations of the X-IFU detector response, we generate spectra with ALP–photon conversion included, and spectra without ALP–photon conversion. We fit all data sets to the model without ALPs (Model 0) and compare the reduced chi-squared of data including ALPs to the reduced chi-squareds of data without ALPs. To allow for the uncertainty in the magnetic field configuration along the line of sight, we repeat this analysis using many different randomly generated magnetic fields.

The two photon spectra that we model are:

(i) Model 0: an absorbed power law plus thermal background:

$$F_0(E) = (AE^{-\gamma} + \mathtt{BAPEC}) \times \mathrm{e}^{-n_\mathrm{H}\sigma(E,z)}, \quad (5)$$

where A and γ are the amplitude and index of the power law, respectively, E is the energy, n_H is the equivalent hydrogen column, $\sigma(E, z)$ is the photoelectric cross-section at redshift z and BAPEC is the standard plasma thermal emission model.

(ii) Model 1: an absorbed power law plus thermal background, multiplied by a table of survival probabilities for photons of different energies:

$$F_1(E, \boldsymbol{B}) = (AE^{-\gamma} + \mathtt{BAPEC}) \times e^{-n_\mathrm{H}\sigma(E,z)} \times P_{\gamma\to\gamma}(E(1+z), \boldsymbol{B}, g_{a\gamma\gamma}). \quad (6)$$

The index of the power law was set based on the best-fitting value from the cleanest *Chandra* observations of NGC 1275, and its normalization was determined based on the *Hitomi* 230 ks observation of Perseus in 2016 (Aharonian et al. 2017). As the AGN in 2016 was roughly twice as bright as in 2009 and it has previously exhibited large historical variation (Fabian et al. 2015), it may be again much brighter (or dimmer) in 2028, which would affect both the contrast against the cluster background and also the observation time required to achieve a certain constraint on $g_{a\gamma\gamma}$.

The 2016 *Hitomi* observation also constrained the temperature, abundances and velocity dispersion of the cluster thermal emission to a high degree of accuracy (Aharonian et al. 2017). For the spectral shape of the cluster background, we used the single-temperature `bapec` model that was a good fit to the *Hitomi* spectrum across its field of view. While this single-temperature model is unlikely to be a good fit for the background contiguous to the AGN, it represents a useful proxy for the actual background that can only be determined at the time. The normalization of the background was set by extracting a circular region of the cluster emission close to the AGN from the *Chandra* observations, of radius equal to the angular resolution of *Athena*, and determining the best fit. All model parameters are shown in Table 2.

As for the study with *Chandra*, we take the central magnetic field value as $B_0 \sim 25\mu$G, following (Taylor et al. 2006). We also assume that B decreases with radius as $B \propto n_e^{0.7}$. As there is not

[1] http://www.the-athena-x-ray-observatory.eu/images/AthenaPapers/The_Athena_Mission_Proposal.pdf
[2] http://cxc.harvard.edu/proposer/POG/html/chap6.html

Table 2. Parameters of the absorbed power law describing the spectrum of NGC 1275, and the thermal model of the cluster background.

Model	Parameter	Symbol	Value
`zwabs`	nH column density	$n_{\rm H}$	$0.24 \times 10^{22}\rm{cm}^{-2}$
	Redshift	z	0.0176
`powerlaw`	Index	γ	1.8
	Normalization	A	9×10^{-3}
`bapec`	Temperature	kT	3.48 keV
	Abundances		0.54 solar
	Velocity dispersion	v	$178\ \rm{m\ s}^{-1}$
	Normalization	N	9×10^{-4}

a direct measurement of the power spectrum and coherence length for the Perseus magnetic field, we base the model on those inferred for the cool core cluster A2199 (Vacca et al. 2012).

The electron density $n_{\rm e}$ has the radial distribution found in (Churazov et al. 2003):

$$n_{\rm e}(r) = \frac{3.9 \times 10^{-2}}{\left[1 + \left(\frac{r}{80\,\rm kpc}\right)^2\right]^{1.8}} + \frac{4.05 \times 10^{-3}}{\left[1 + \left(\frac{r}{280\,\rm kpc}\right)^2\right]^{0.87}}\ \rm{cm}^{-3}. \qquad (7)$$

The magnetic field is generated over 300 domains, whose lengths are drawn from a Pareto distribution between 3.5 and 10 kpc with power 2.8. In each domain, the magnetic field and electron density are constant, with a random direction of $\boldsymbol{B}$. We then calculate the survival probability of a photon passing through this region, as described in (Angus et al. 2014).

The simulations were performed using the Simulation of X-ray Telescopes (SIXTE) code, a multi-instrument simulation package. It aims to offer an end-to-end simulation, i.e. the full detector chain from the source to the final data. It models the telescope's vignetting, ARF and PSF, and X-IFU's response, event reconstruction and pile-up (Wilms et al. 2014).

The spectrum of NGC 1275, and the cluster background, were modelled in XSPEC[3] as an absorbed power law plus a thermal component, `zwabs` ∗ (`powerlaw` + `bapec`). This spectrum, either multiplied with the photon survival probabilities or not, was converted to the SIMPUT[4] file format using the command `simputfile`. The mirror and detector response were modelled with `xifupipeline`, using the ARF file athena_xifu_1469_onaxis_pitch249um_v20160401.arf and the RMF file athena_xifu_rmf_v20160401.rmf. This generated an event FITS file, which was then converted into a PHA file using `makespec`. We produced a fit to this spectrum in XSPEC, using the Levenberg–Marquardt fitting method to calculate the reduced χ^2. Fig. 2 shows one simulation for $g_{a\gamma\gamma} = 3 \times 10^{-13}\rm{GeV}^{-1}$ and its fit to an absorbed power law.

We use the following procedure to determine whether a particular value of $g_{a\gamma\gamma}$ is excluded: we varied the ALP–photon coupling $g_{a\gamma\gamma}$ from $g_{a\gamma\gamma} = 5 \times 10^{-13}\ \rm{GeV}^{-1}$ to $g_{a\gamma\gamma} = 1 \times 10^{-13}\ \rm{GeV}^{-1}$, with step size $0.5 \times 10^{-13}\ \rm{GeV}^{-1}$. As the bound is dependent on uncertainties in the magnetic field strength of a factor of 2, and we are only using simulated data, we do not consider step sizes smaller than this. For each $g_{a\gamma\gamma}$:

(i) Generate 50 configurations of the magnetic field B_i.

(ii) Use the B_i to calculate the survival probability $P_{\gamma\to\gamma}$ along the line of sight for different photon energies (as done in Angus et al. 2014). We calculate for 8000 equally spaced photon energies in the range 0.01–10 keV.

(iii) Combine each $P_{\gamma\to\gamma}$ with the AGN spectrum.

(iv) Generate 10 fake PHAs for each spectrum, providing 500 fake data samples in total.

(v) Fit the fake data to Model 0, and calculate the reduced chi-squared χ^2_1.

(vi) Generate 100 fake PHAs based on Model 0, and compute the average of their reduced chi-squareds χ^2_0. Assuming the absence of ALPs, this represents the expected quality of the fit to the single real data set. If the actual data are a poor fit for some reason, then this will weaken the level of the resulting bounds that we can produce.

(vii) Determine the percentage of fake data sets that have a reduced chi-squared $\chi^2_1 < \max(\langle\chi^2_0\rangle, 1)$. If this is true for less than 5 per cent of the data sets, the value of $g_{a\gamma\gamma}$ is excluded at 95 per cent confidence.

[3] https://heasarc.gsfc.nasa.gov/xanadu/xspec/manual/manual.html

[4] http://hea-www.harvard.edu/heasarc/formats/simput-1.0.0.pdf

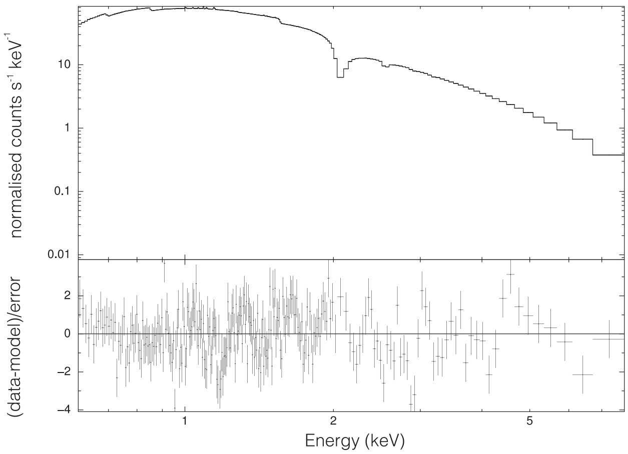

Figure 2. A simulated 200 ks data set for NGC 1275 with $g_{a\gamma\gamma} = 3 \times 10^{-13}\rm{GeV}^{-1}$, and its fit to Model 0. The characteristic ALP-induced modulations are apparent.

For a simulation of 200 ks of data with the nominal mirror configuration, we derive a projected bound of $g_{a\gamma\gamma} \lesssim 1.5 \times 10^{-13}\rm{GeV}^{-1}$ at 95 per cent confidence and of $g_{a\gamma\gamma} \lesssim 2.5 \times 10^{-13}\rm{GeV}^{-1}$ at 99 per cent confidence, as shown in Fig. 3 alongside published data limits. This represents an order of magnitude improvement over the bound derived from the 200 ks of *Chandra* ACIS-I observations in (Berg et al. 2017). We also find that even a short 10 ks observation will lead to an improved bound of $g_{a\gamma\gamma} \lesssim 4.5 \times 10^{-13}\rm{GeV}^{-1}$.

These bounds are substantially better than any current experimental or astrophysical bound, and also go beyond the capabilities of IAXO for ultralight ALP masses. The proposed DM haloscope ABRACADABRA has the potential to explore $g_{a\gamma\gamma}$ down to $10^{-17}\rm{GeV}^{-1}$ for $m_{\rm a} \in [10^{-14}, 10^{-6}]$eV (Kahn, Safdi & Thaler 2016), if ALPs constitute the dark matter. The existence of ALP-induced oscillations in galaxy clusters is independent of this. Proposed CMB experiments such as PIXIE (Kogut et al. 2011) and PRISM (Andre et al. 2013) could produce a constraint $g_{a\gamma\gamma}B < 10^{-16}\rm{GeV}^{-1}nG$, which might be competitive with bounds from galaxy clusters if the cosmic magnetic field is close enough to saturation ∼nG (Tashiro, Silk & Marsh 2013). Black hole superradiance also offers tentative constraints ALPs in the mass range $m_{\rm a} \in [10^{-14}, 10^{-10}]$eV, depending on measurements of black hole spin (Arvanitaki et al. 2017).

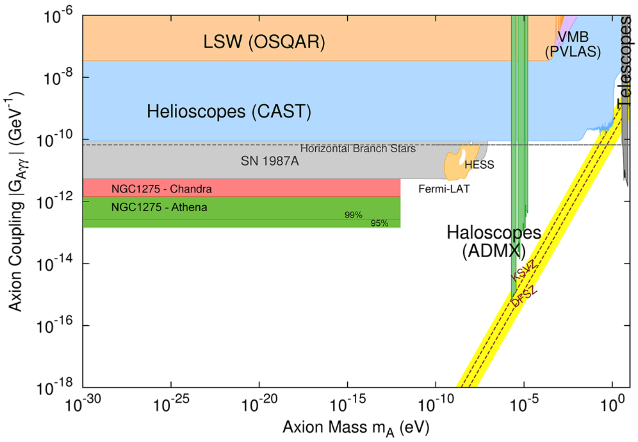

Figure 3. Overview of exclusion limits on axion couplings versus mass. For axion masses $m_a \sim 10^{-12}$eV then ALP–photon conversion can enter a resonant regime, with the potential of stronger bounds around this critical mass. We do not perform a detailed study of the resonant regime in this work and focus only on the low-mass region. Full references can be found in the Particle Data Group review on *Axions and other similar particles* (Patrignani et al. 2016).

5 CONCLUSION

AGNs situated in galaxy clusters are excellent targets to search for ALP–photon interconversion. *Athena*'s groundbreaking new technology will be able to resolve AGN spectra very precisely. The bound $g_{a\gamma\gamma} \lesssim 1.5 \times 10^{-13}\text{GeV}^{-1}$ derived from simulations of 200 ks observations is an order of magnitude improvement over the bounds from current generation satellites. For the mass range $m_a \lesssim 10^{-12}$eV, it will also be far better than the bounds obtainable from future experimental searches such as IAXO.

We stress that this is only a first estimate of the sensitivity of *Athena* to ALP-induced modulations. The final sensitivity will depend on the capabilities of the finished satellite, the brightness of the AGN in 2028 and the quality of the actual data. Telescopes such as the Square Kilometre Array (SKA) are likely to reduce the uncertainties in the magnetic field model (Braun et al. 2015), allowing for greater precision in $g_{a\gamma\gamma}$ bounds calculations by the time *Athena* launches. However, we have demonstrated that *Athena* will certainly improve bounds on $g_{a\gamma\gamma}$ substantively, and that X-ray astronomy will continue to be at the forefront of ultralight ALP searches in the coming decades.

ACKNOWLEDGEMENTS

This project is funded in part by the European Research Council starting grant 'Supersymmetry Breaking in String Theory' (307605). Both Francesca Day and Nicholas Jennings are also funded by STFC.

REFERENCES

Aharonian F. A. et al., 2017, ApJ, 837, L15
Ajello M. et al., 2016, Physical Review Letters, 116, 161101
Andre P. et al., 2013, preprint (arXiv:1306.2259)
Angus S., Conlon J. P., Marsh M. C. D., Powell A. J., Witkowski L. T., 2014, J. Cosmol. Astropart. Phys., 1409, 026
Arvanitaki A., Baryakhtar M., Dimopoulos S., Dubovsky S., Lasenby R., 2017, Phys. Rev., D95, 043001
Balmaverde B., Capetti A., Grandi P., 2006, A&A, 451, 35
Barret D. et al., 2016, in den Herder J.-W. A., Takahashi T., Bautz M., eds, Proc. SPIE Conf. Ser. Vol. 9905, Space Telescopes and Instrumentation 2016: Ultraviolet to Gamma Ray. SPIE, Bellingham, p. 99052F
Berg M., Conlon J. P., Day F., Jennings N., Krippendorf S., Powell A. J., Rummel M., 2017, ApJ, 847, 101
Boyarsky A., Ruchayskiy O., Iakubovskyi D., Franse J., 2014, Phys. Rev. Lett., 113, 251301
Braun R., Bourke T., Green J. A., Keane E., Wagg J., 2015, PoS, AASKA14, 174
Bulbul E., Markevitch M., Foster A., Smith R. K., Loewenstein M., Randall S. W., 2014, ApJ, 789, 13
Burrage C., Davis A.-C., Shaw D. J., 2009, Phys. Rev. Lett., 102, 201101
Churazov E., Forman W., Jones C., Bohringer H., 2003, ApJ, 590, 225
Cicoli M., Goodsell M., Ringwald A., 2012, J. High Energy Phys., 10, 146
Conlon J. P., 2006, J. High Energy Phys., 05, 078
Conlon J. P., Marsh M. C. D., 2013, Phys. Rev. Lett., 111, 151301
Conlon J. P., Powell A. J., Marsh M. C. D., 2016, Phys. Rev. D, 93, 123526
Conlon J. P., Day F., Jennings N., Krippendorf S., Rummel M., 2017, J. Cosmol. Astropart. Phys., 1707, 005
Fabian A. C., Walker S. A., Pinto C., Russell H. R., Edge A. C., 2015, MNRAS, 451, 3061
Gottardi L. et al., 2014, in Takahashi T., den Herder J.-W. A., Bautz M., eds, Proc. SPIE Conf. Ser. Vol. 9144, Space Telescopes and Instrumentation 2014: Ultraviolet to Gamma Ray. SPIE, Bellingham, p. 91442M
Irastorza I. G. et al., 2012, in Zioutas K., Schumann M., eds, Proc. 7th Patras Workshop on Axions, WIMPs and WISPs (AXION-WIMP 2011): Mykonos, Greece, June 27-July 1, 2011. p. 98, available at http://inspirehep.net/record/1084988/files/arXiv:1201.3849.pdf
Kahn Y., Safdi B. R., Thaler J., 2016, Phys. Rev. Lett., 117, 141801
Kogut A. et al., 2011, J. Cosmol. Astropart. Phys., 1107, 025
Marsh M. C. D., Russell H. R., Fabian A. C., McNamara B. P., Nulsen P., Reynolds C. S., 2017, preprint (arXiv:1703.07354)
Mirizzi A., Redondo J., Sigl G., 2009, J. Cosmol. Astropart. Phys., 0908, 001
Nandra K. et al., 2013, preprint (arXiv:1306.2307)
Patrignani C. et al., 2016, Chin. Phys., C40, 100001
Payez A., Evoli C., Fischer T., Giannotti M., Mirizzi A., Ringwald A., 2015, J. Cosmol. Astropart. Phys., 1502, 006
Peccei R. D., Quinn H. R., 1977, Phys. Rev. Lett., 38, 1440
Raffelt G., Stodolsky L., 1988, Phys. Rev., D37, 1237
Ringwald A., 2012, Phys. Dark Univ., 1, 116
Sikivie P., 1983, Phys. Rev. Lett., 51, 1415
Svrcek P., Witten E., 2006, J. High Energy Phys., 06, 051
Tashiro H., Silk J., Marsh D. J. E., 2013, Phys. Rev., D88, 125024
Taylor G. B., Gugliucci N. E., Fabian A. C., Sanders J. S., Gentile G., Allen S. W., 2006, MNRAS, 368, 1500
Vacca V., Murgia M., Govoni F., Feretti L., Giovannini G., Perley R. A., Taylor G. B., 2012, A&A, 540, A38
Weinberg S., 1978, Phys. Rev. Lett., 40, 223
Wilczek F., 1978, Phys. Rev. Lett., 40, 279
Wilms J. et al., 2014, in Takahashi T., den Herder J.-W. A., Bautz M., eds, Proc. SPIE Conf. Ser. Vol. 9144, Space Telescopes and Instrumentation 2014: Ultraviolet to Gamma Ray. SPIE, Bellingham, p. 91445X
Wouters D., Brun P., 2013, ApJ, 772, 44
Yamazaki S. et al., 2013, Publ. Astron. Soc. Japan, 65

This paper has been typeset from a TEX/LATEX file prepared by the author.